

RADIO AND WHITE-LIGHT CORONAL SIGNATURES ASSOCIATED WITH THE *RHESSI* HARD X-RAY EVENT OF 2002 JULY 23

M. J. REINER¹

Catholic University of America, Washington, DC; and NASA Goddard Space Flight Center, Greenbelt, MD

S. KRUCKER

Space Sciences Laboratory, University of California, Berkeley, CA

D. E. GARY

Center for Solar-Terrestrial Research, New Jersey Institute of Technology, Newark, NJ

B. L. DOUGHERTY

Los Alamos National Laboratory, Los Alamos, NM

M. L. KAISER

Space Weather Laboratory, NASA Goddard Space Flight Center, Greenbelt, MD

AND

J.-L. BOUGERET

LESIA, Observatoire de Paris, Meudon, France

Received 2006 January 25; accepted 2006 November 10

ABSTRACT

Simultaneous radio, white-light, and hard X-ray (HXR) observations for the 2002 July 23 γ -ray flare event are used to establish the relationship of a complex type III-like burst to the corresponding coronal mass ejection (CME) and the coronal electron acceleration signatures observed in the decimeter/microwave (dm-cm) emissions and X-rays. We find that the onset of the type III-like emissions for this event is coincident with the impulsive *RHESSI* HXR event, the dm-cm radio emissions and with the linearly extrapolated liftoff time of the CME. The overall intensity-time characteristics of the complex type III-like burst resembles that of both the dm-cm flux and the HXR light curve that correspond to an electron acceleration event deep in the corona. Furthermore, the complex radiation characteristics of the type III-like emissions are found to be directly related to the CME kinematics, which is directly related to the frequency drift of the associated low-frequency (kilometric) type II emissions. The frequency-drift characteristics of the high-frequency (metric) type II emissions observed for this event, on the other hand, are not clearly related to the kilometric type II emissions and therefore to the observed CME height-time characteristics, indicating that these emissions may correspond to an independent coronal shock wave.

Subject headings: Sun: activity — Sun: corona — Sun: flares — Sun: radio radiation — Sun: X-rays, gamma rays — solar-terrestrial relations

1. INTRODUCTION

The 2002 July 23 solar energetic event was the first γ -ray flare observed by the NASA *RHESSI* and has been extensively analyzed (e.g., see Lin et al. 2003 and references therein). Most of these initial studies focused on the observations of phenomena that occurred very near the solar surface and that therefore directly relate to the hard X-ray (HXR) and γ -ray event observed by *RHESSI*. The association of the HXR and γ -ray events to the corresponding complex type III-like burst and the associated CME, both of which correspond to phenomena occurring much higher in the corona, was not fully addressed in those initial papers.

The low-frequency type III-like emissions associated with this event were very intense and complex and of uncommonly long duration. Such type III-like emissions (previously called SA events) were extensively studied in the 1980s (Cane et al. 1981; Cane & Stone 1984; Kundu & Stone 1984; Kundu et al. 1990; Kahler et al. 1986, 1989; MacDowall et al. 1987). More recently, *Wind* WAVES made the first full frequency observation

of an SA event (Bougeret et al. 1998). In addition, Reiner & Kaiser (1999a) found that such complex bursts often have unusual radiation characteristics in the 1–14 MHz band. These radiation characteristics include signatures that suggest multiple injections of the exciter electrons that produce this radiation, a characteristic diminution of flux density between 3 and 10 MHz, and some very narrow band features of short duration (minutes) that appear to have little or no measurable frequency drift. By contrast, ordinary type III radio bursts display signatures of a single injection and a relatively uniform intensity structure across this frequency band. Because of these unusual radiation characteristics, Reiner & Kaiser (1999a) referred to such emissions as complex type III-like emissions to distinguish them from the more common type III bursts associated with solar flares and subflares (usually without accompanying CMEs).

Since these complex type III-like emissions are signatures of major solar events involving CMEs and possibly solar energetic particles (SEPs), they can therefore provide an early-warning signature of a possible space weather event, even before the corresponding CME is observed in the LASCO coronagraph. Hence, they can be used as a proxy for such events. To be able to correctly identify these events and to be able to distinguish them

¹ Also at NASA/GSFC, Code 695, Greenbelt, MD.

from ordinary type III radio bursts, it is therefore necessary to understand the physical origin and nature of their unusual radiation characteristics.

To gain insights into the origin of these complex emissions, Reiner et al. (2000b) compared the 1 MHz radio flux densities with the decimeter/microwave (dm–cm) emissions near 4.5 GHz, which are believed to be signatures of electron acceleration deep in the corona. They found that the complex type III–like events, unlike the ordinary type III bursts, were often well correlated both in time and intensity profile to the dm–cm emissions. They therefore concluded that the complex type III emissions were likely produced by electrons accelerated deep in the corona, near the flare site (also see Cane et al. 2002). Such observations also provide a qualitative explanation for the multiple injection signatures of the radiation for these events.

While these observations provided insights into the origin of these emissions, they did not explain the other unusual radiation characteristics, such as the diminished radiation and the narrow-band features. The physical origin of these radiation characteristics is not yet fully understood. Reiner & Kaiser (1999a) speculated that these features may result from the propagation of the exciter electron beam through the turbulent, inhomogeneous region in the vicinity of an overlying CME. Indeed, Reiner et al. (2001) found that these complex type III–like emissions were generally associated with major solar flare events with accompanying CMEs. This gave further support to the idea that the unusual radiation characteristics of these emissions were related to CMEs.

The purpose of this paper is to investigate how the radiation characteristics of the low-frequency radio emissions for the July 23 γ -ray flare event relate to the phenomena observed near the solar surface, as revealed by the high-frequency radio and HXR emissions, and to the kinematics of the CME, corresponding to phenomena in the high corona. It will be demonstrated that the frequency range of the diminished radiation intensity is consistent with the propagation of the flare-accelerated electrons through the turbulent region of the overlying CME.

2. DESCRIPTION OF INSTRUMENTS USED IN THIS INVESTIGATION

The primary instruments used in this investigation were the space-based *Wind* WAVES and the ground-based Hiraiso Radio Spectrograph (HiRAS) and Solar Radio Burst Locator (SRBL) radiospectrographs. The white-light observations were made by the *Solar and Heliospheric Observatory* (SOHO) LASCO coronagraph, and the HXR were obtained from *RHESSI*.

The WAVES instrument on the *Wind* spacecraft includes several radio receivers that cover the frequency range from 4.0876 kHz to 13.825 MHz (Bougeret et al. 1995). The instruments used in the present analysis were two superheterodyne (step-tuned) receivers. The high-frequency (RAD2) receivers sweep 256 frequency channels from 1.075 to 13.825 MHz in 16.192 s, with a frequency resolution of 50 kHz and a bandwidth of 20 kHz. The low-frequency (RAD1) receivers cover the frequency range from 20 to 1040 kHz at 32 discrete frequencies (selected from 256 frequency channels) with a highest sampling rate of 45.8 s and a bandwidth of 3 kHz. At the time of the observations presented here the *Wind* spacecraft was $33 R_{\oplus}$ from Earth, at (25.0, 22.0, 1.7) R_{\oplus} geocentric solar ecliptic (GSE), during one of its distant prograde orbits.

The ground-based HiRAS, located near Hiraiso, Japan, has been continuously monitoring solar radio emissions in the frequency range from 25 MHz to 2.5 GHz since 1993, with a time resolution of 3 to 4 s (Kondo et al. 1995). It consists of three

antennas covering the frequency ranges from 25 to 70, from 70 to 500, and from 500 to 2500 MHz, respectively. The SRBL, located at the Owens Valley Radio Observatory, is an automated, ground-based instrument developed by Caltech and currently operated by the New Jersey Institute of Technology (NJIT) Center for Solar-Terrestrial Research. The instrument, consisting of a 6 foot parabolic dish, acquires spectra of solar activity to 18 GHz, scanning through 120 frequencies every 4.8 s (Dougherty et al. 2000). The data resolution used here was 9.6 s.

The LASCO coronagraph on the *SOHO* spacecraft has three optical systems with overlapping and concentric fields of view (Brueckner et al. 1995). The *SOHO* spacecraft is located at L1 from where it has continuously monitored the Sun since 1995. The analyses in this paper use images recorded on 2002 July 23 with the C2 (2–7 R_{\odot}) and C3 (3.7–32 R_{\odot}) coronagraphs. The nominal C2 image cadence is 24 minutes.

The NASA *RHESSI*, launched on 2002 February 5, provides high-resolution imaging and spectroscopy of X-rays and γ -rays from 3 keV to 17 MeV (Lin et al. 2002).

3. OBSERVATIONS

3.1. Overview of the 2002 July 23 Event

On 2002 July 23 *GOES* observed an X4.8 soft X-ray long-duration event (LDE), shown in Figure 1a, that began at \sim 00:18 UT and reached maximum intensity by 00:35 UT. An associated 2B H α flare was observed in NOAA 0039, located at S13 $^{\circ}$, E72 $^{\circ}$, from 00:23 to 02:40 UT, with maximum at 00:29 UT. This event was accompanied by a fast CME, observed by *SOHO* LASCO, originating from the same active region. The *RHESSI* hard X-ray (HXR) flux observed for this event exhibited a rise phase (from \sim 00:18 to \sim 00:27 UT) followed by an intense impulsive phase (from \sim 00:27 to \sim 00:43 UT) (Krucker et al. 2003; Lin et al. 2003). The total *RHESSI* HXR flux for this event is also plotted in Figure 1a.

An overview of the low-frequency radio emissions observed for this event is presented in the dynamic spectrum in Figure 1b, which displays the intensity of the radio emissions (mauve being the most intense) measured by the RAD1 and RAD2 *Wind* WAVES radio receivers from 00:00 to 04:00 UT on 2002 July 23 in the frequency range between 125 kHz and 13.825 MHz. As is typical, this major flare/CME solar event produced an intense, complex type III–like burst (Reiner & Kaiser 1999a), with onset at 00:27 UT, that extended from the highest observing frequency of 13.825 MHz to the local plasma frequency near 20 kHz at the *Wind* spacecraft (not shown). (In Fig. 1b the intense type III–like radio emissions are overexposed in order to make the very weak type II radio emissions, discussed below, more visible.) These intense, complex type III–like emissions, with the same onset time as the impulsive *RHESSI* HXR event, lasted nearly 35 minutes, until about 01:00 UT—similar to the duration of the HXR event.

In addition to the intense, complex type III–like emissions, there were much weaker slowly frequency-drifting type II radio emissions visible on the dynamic spectrum, especially below 1 MHz. (At frequencies below a few hundred kHz, these weak type II emissions are obscured by the more intense aurora kilometric radiation [AKR] that is generated in Earth's auroral region; Gurnett 1975.) Kilometric type II emissions are known to be generated by electrons accelerated at CME-driven shocks, as they propagate through the interplanetary medium (Cane et al. 1987; Bale et al. 1999); their frequency drift rate is directly related to the speed of the CME-driven shock (e.g., see Reiner et al. 1998). Hence, the type II emissions for the July 23 event

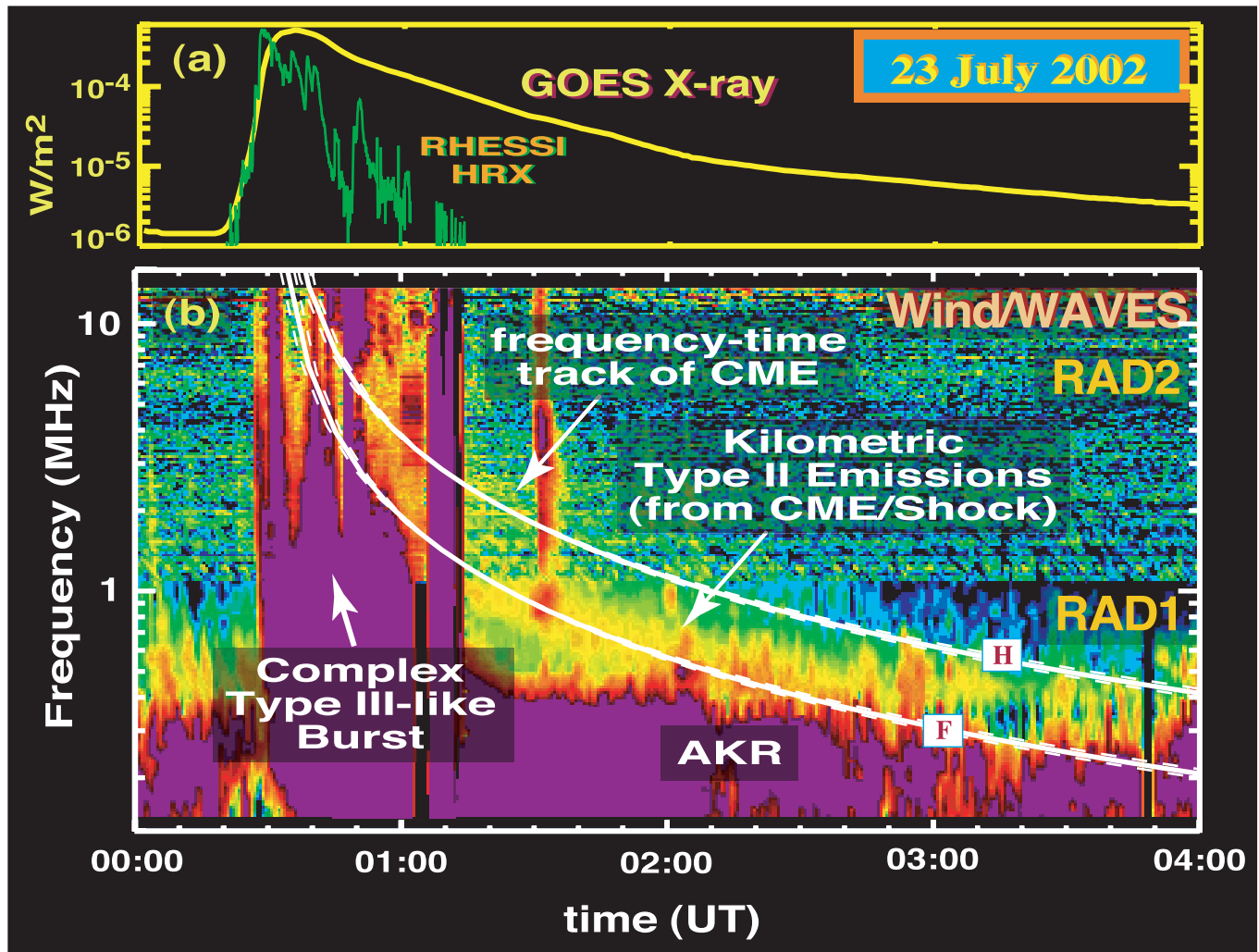


FIG. 1.—Overview of the X-ray and low-frequency radio emissions associated with the 2002 July 23 X4.8 LDE X-ray event. (a) *GOES* soft X-ray and *RHESSI* HXR emissions observed from 00:00 to 04:00 UT. (b) Radio dynamic spectrum in the frequency range from 125 kHz to 13.8 MHz, over the same time period, showing the intense, complex type III-like emissions (overexposed) associated with the flare and the slowly frequency-drifting type II emissions generated by the propagation of the associated CME through the interplanetary medium. The solid and dashed curves on the dynamic spectrum correspond to the frequency-time track of the CME, generating radio emissions at the fundamental and harmonic of the plasma frequency.

were generated by a shock driven by the associated CME within and beyond the *LASCO* field of view.

3.2. Connection between High- and Low-Corona Phenomena Implied by the Radio and X-Ray Emissions

The complexity of the type III emissions at decametric and hectometric (Dm–Hm) wavelengths (1–14 MHz), associated with this X-class flare/CME event, are more clearly revealed, at higher time resolution (18 s), in the dynamic spectrum in Figure 2a. As is typical for such events, these complex type III-like radio emissions, which commenced at 00:27 UT, consist of what appear to be distinct multiple type III bursts, suggesting multiple electron ejections, that coalesce at frequencies below ~ 3 MHz into intense frequency-drifting substructures that extend to very low frequencies. While the intensity of the initial component type III burst at about 00:31 UT is approximately uniform across this frequency band, there is a clear diminution in the emission intensity between about 3 and 14 MHz for the subsequent components of this complex type III event. In fact, the re-intensification of the emissions appears to occur at lower and lower frequencies with time, more or less following the white curves (to be explained below). Finally, at frequencies below

about 3 MHz, particularly after about 00:50 UT, there are some very narrowband (~ 50 – 100 kHz) features of short duration (minutes) that appear to have little or no measurable frequency drift.

In Figure 2 we also display, on the same logarithmic scale, the higher frequency radio data that correspond to physical phenomena occurring low ($\leq 2 R_{\odot}$) in the corona. The *HiRAS* dynamic spectrum in Figure 2b, which extends the frequency coverage from 25 MHz to 2.5 GHz, shows that there were also complex metric type II emissions from $\sim 00:29$ to 00:55 UT at frequencies below ~ 300 MHz, and metric type IV (continuum) emissions from 00:29 to $\sim 00:45$ UT at frequencies centered at about 500 MHz. In addition, there were some metric type III emissions that appear to be the high-frequency continuation of several of the multiple components that constitute the complex Dm–Hm type III-like burst.

Figure 3b shows a dynamic spectrum of the *SRBL* data in the frequency band from 2 to 18 GHz, from 00:25 to 00:55 UT. This intense radio event, with sudden onset also at about 00:27 UT, continues beyond 1 UT and shows an intensity-time structure that is more or less uniform across its frequency range. Profiles of the radio flux density obtained from this dynamic spectrum

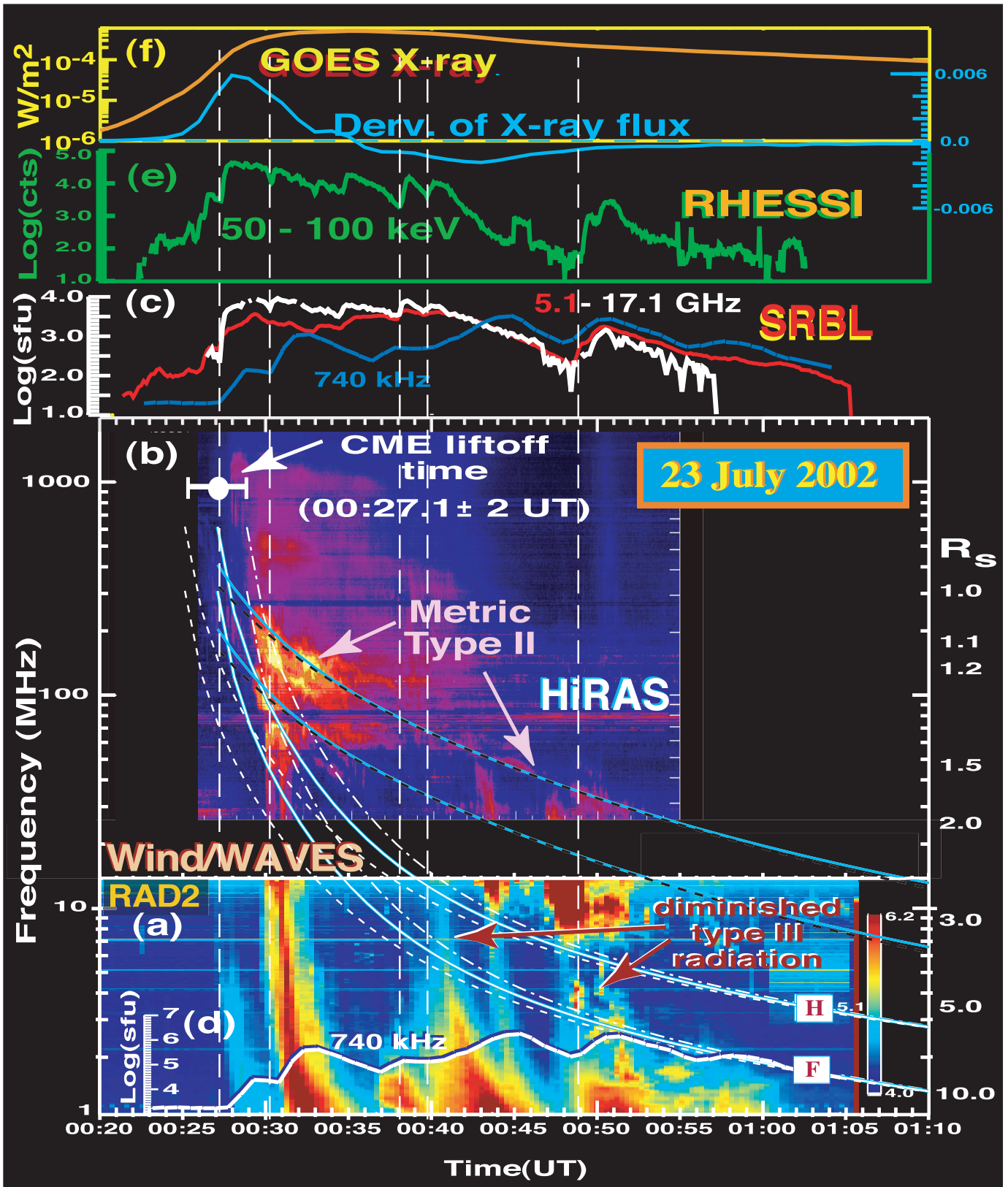


FIG. 2.— (a) High-frequency/time resolution *Wind* WAVES dynamic spectrum from 00:20 to 01:10 UT in the frequency range from 1 to 13.8 MHz showing, in more detail, the complexity of the type III radio emissions. (b) The HiRAS dynamic spectrum in the frequency range from 25 MHz to 2.5 GHz showing the metric type II, type III, and type IV radio emissions associated with this event. (c) The intensity profiles of the radio emissions measured by SRBL at 5.1 and 17.1 GHz and superposed flux density at 0.74 MHz. (d) The intensity-time profile of the radio emissions at 0.75 MHz. (e) The light curves of the various HXR sources observed by *RHESSI*. (f) The *GOES* soft X-ray flux (orange curve) and the derivative of this flux (blue curve). The curves overlying the dynamic spectra (explained in the text) correspond to the frequency-time tracks of various possible coronal and CME-driven shocks associated with this event. Note that the projected liftoff time of the CME corresponds, to within the measurement uncertainties, to the onset of the impulsive *RHESSI* HXR event and sudden rise in the 2.5–17.1 GHz radio flux indicating a significant particle acceleration event.

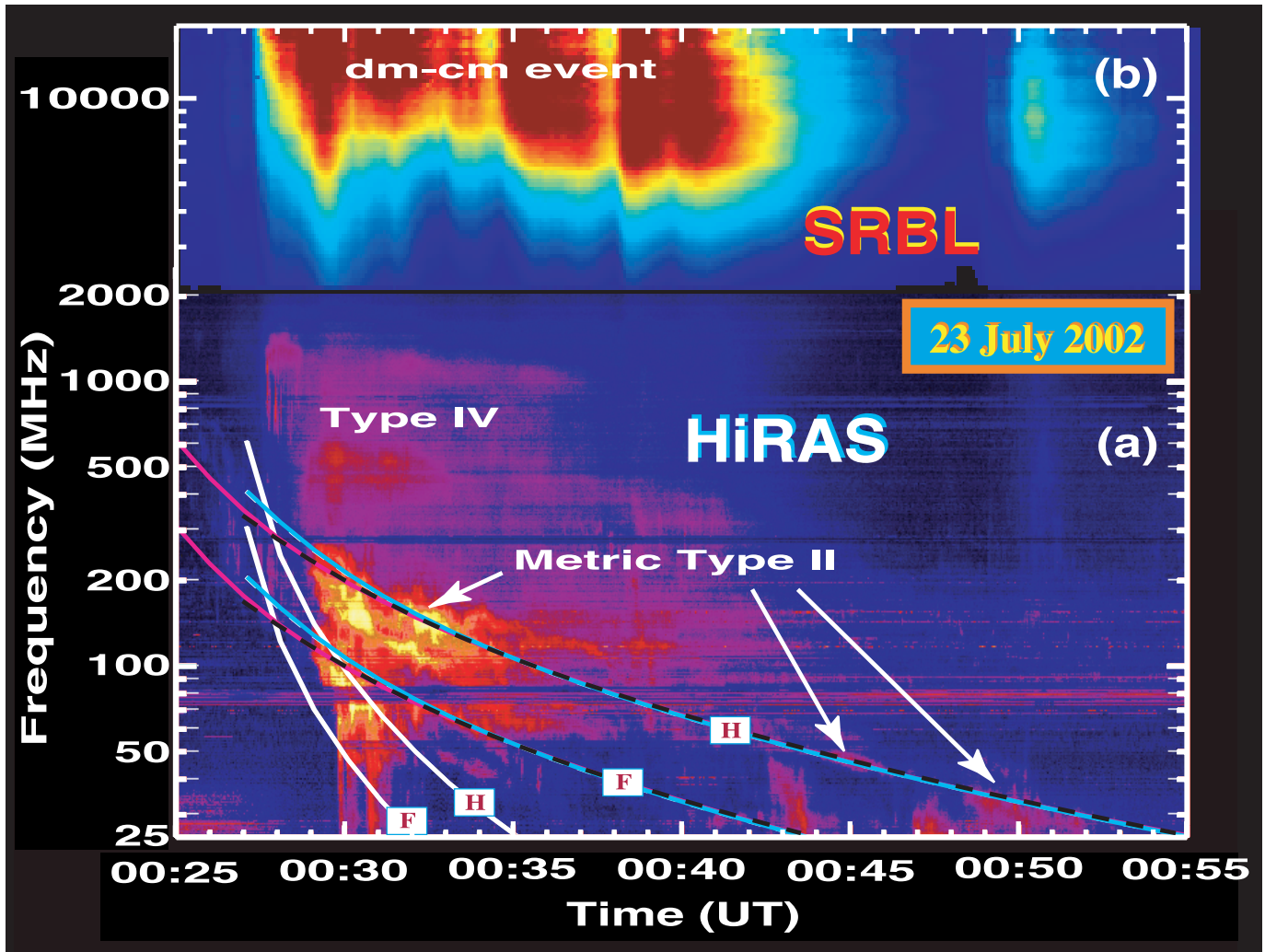


FIG. 3.—(a) Details of the HiRAS dynamic spectrum from 00:25 to 00:55 UT in the frequency range from 25 MHz to 2.5 GHz. Overlaid on this dynamic spectrum are the various frequency-time tracks corresponding to the various shock dynamics as shown in Fig. 3 and explained in the text. (b) Dynamic spectrum of the SRBL radio data from 2 to 18 GHz.

at 5.1 and 17.1 GHz are plotted in Figure 2c (red and white curves). For comparison, we also show in Figures 2c and 2d the flux density of the complex type III-like emissions observed at 0.74 MHz, the frequency at which the various multiple components of the complex type III merged together.

The soft X-ray (SXR) flux (orange curve) and its time derivative (blue curve) are shown in Figure 2f. It is well known that, for large impulsive flares, sudden changes in the derivative of the soft X-ray flux are related to nonthermal electron injections (Neupert effect), as evidenced by the hard X-rays and impulsive microwave events (Neupert 1968; Dennis & Zarro 1993). A sudden change in derivative of the SXR flux occurs at about 00:27 UT, suggesting a significant electron acceleration event in the low corona. Lin et al. (2003) pointed out that for the July 23 event the GOES soft X-ray time profile during the rise phase is similar to the time integral of the RHESSI HXR (12–25 keV) flux, thereby confirming the Neupert effect for this event.

Direct evidence for an electron acceleration event deep in the corona is provided by the HXR flux. The total RHESSI HXR flux [in log (counts)] at 50–100 keV is presented in Figure 2e. Figures 2e and 2f show a temporal correspondence between the sudden change in the derivative of the SXR flux and the impulsive phase of the RHESSI HXR flux. Krucker et al. (2003) have shown that

the impulsive HXR sources, which commenced at 00:27:27.0 UT, were located at the footpoints of coronal magnetic loops.

Spikes in the RHESSI HXR flux profile indicate secondary electron injections at about 00:30, 00:35, 00:38, 00:40, 00:49 and 00:50 UT. In Figure 2 we indicated the times of several of these secondary injections with vertical dashed lines. White et al. (2003) pointed out the good correspondence between the spikes and dips in the HXR and microwave radio flux at 35 GHz to 00:45 UT for this July 23 event. The comparison of the RHESSI HXR light curve and the 17.1 GHz radio flux in Figures 2c and 2e shows that this similarity extends even beyond 00:45 UT. While this resemblance is significantly less pronounced in the 5.1 GHz flux, nevertheless many of the peaks in the HXR and 17.1 GHz fluxes are also reflected in the 5.1 GHz profile. The dissimilarities in the radio profiles at lower frequencies are expected and are due mainly to a combination of energy-dependent trapping (producing smoother profiles at lower frequencies) and to optical depth effects.

The impulsive RHESSI HXR event, the sudden increase in the 5.1–17.1 GHz radio flux and the sudden change in derivative of the SXR flux all signify a significant electron acceleration event in the low corona beginning at about 00:27 UT, well after the onset of the flare and initial HRX event at 00:18 UT. The onset of

this major electron acceleration event occurs at precisely the onset time of the dekametric-to-kilometric type III emissions that signal the escape of electrons into interplanetary space. Furthermore, it is significant that the *RHESSI* impulsive event and the dm–cm radio emissions encompass the entire duration of the complex type III–like event. Such a good temporal correspondence between the HXR and low-frequency radio emissions is rarely observed for ordinary type III bursts.

As in the previous comparisons with the dm–cm fluxes (Reiner et al. 2000b), the temporal variations also show some similarities in detail. To show this more clearly, we have superposed the 0.74 MHz flux density (*blue curve*) on Figure 2c (shifted by about 1 minute earlier to take into account the electron propagation time up to the plasma level corresponding to the 0.74 MHz emissions). The calculated cross correlation between the 5.1 GHz and 0.74 MHz time series shows a broad peak indicating a correlation of about 0.62.

As indicated by the vertical dashed lines in Figure 2, many of the peaks in the HXR and dm–cm fluxes correspond to sudden changes in the 0.74 MHz flux density. Just as for the comparison between the HXR and microwave emissions, we do not expect a detailed correspondence between the heights of the peaks for the HXR or dm–cm emissions and 0.74 MHz emissions, since the intensity of the radiation generated at a given time and location depends on a number of complex factors. What is more, while both the HXR and microwave emissions were likely produced by a population of downward propagating high-energy (~ 100 keV) electrons, the low-frequency emissions were generated by a different population of escaping lower-energy (~ 10 keV) electrons, propagating through a very different plasma medium. Hence, we also do not necessarily expect a precise correspondence of the injection times. Nevertheless, the observed good qualitative temporal correspondence of the HXR and high-frequency radio emissions to the low-frequency radio emissions strongly suggests that the coronal acceleration process that produced the downward propagating and trapped electrons was at the same time continually producing lower energy electrons that escaped along open interplanetary magnetic field lines, where they generated the complex type III–like emissions.

3.3. Relationship of the CME kinematics to the Low-Frequency Radio Observations

Now that it has been established that this complex type III–like event was likely generated by an electron acceleration event deep in the corona, we would like to understand the origin of the reduced radio flux density observed for these complex type III emissions in the frequency range between 3 and 14 MHz. Since such complex type III–like events are always associated with CMEs and since both of these are high coronal phenomena, we have examined how the kinematics of the associated CME relates to the radiation characteristics of the complex type III emissions.

A very fast east-limb CME was first observed (00:42:05 UT) in the *SOHO* LASCO C2 coronagraph at $3.95 R_{\odot}$. The speed of this CME was such that only two height-time data measurements were available before this CME left the field-of-view of the LASCO coronagraph ($\geq 32 R_{\odot}$). These height-time data are plotted in Figure 4. The weighted (using nominal measurement uncertainties for the C2 and C3 coronagraph measurements) best straight-line fit (Fig. 4, *solid line*) gives a (plane-of-sky) speed of 2285 ± 91 km s $^{-1}$. Since this CME was near the east limb, this measured speed should be close to the actual CME radial speed. The dashed lines in Figure 4 indicate the uncertainties in the CME kinematics derived from these data. Extrapolating this constant-speed fit back to the solar surface at $1 R_{\odot}$

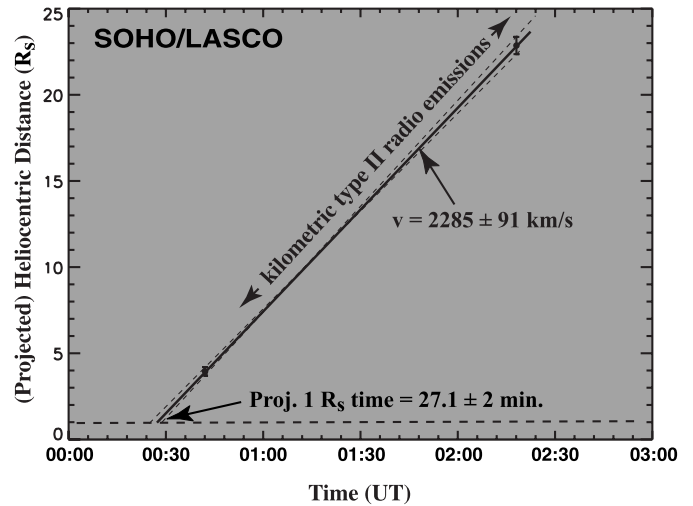


FIG. 4.—Height-time data for the LASCO CME. The solid straight line is the weighted best fit to the height-time measurements and the dashed lines correspond to the uncertainty in the fit.

yields a projected CME liftoff time of $00:27.1 \pm 00:02$ UT. For such a fast CME it is likely that the CME reached its final speed very quickly, without a long gradual acceleration phase (St. Cyr et al. 1999; Reiner et al. 2003). This linearly extrapolated liftoff time is therefore expected to be very close to the actual liftoff time of the CME.

To relate the CME kinematics, displayed on the height-time plot in Figure 4, to the frequency drift rate of the type II emissions shown in Figure 1b, it is necessary to use an appropriate coronal density–distance scale (Reiner et al. 1998), since this is the only means of quantitatively relating radio and white-light phenomena in the high and low corona. The (ion) plasma density in the interplanetary medium for $R \geq 0.3$ AU is known, from direct in situ plasma density measurements, to scale as $1/R^2$, where R is the heliocentric distance (Bougeret et al. 1984). However, the radial distance behavior of the plasma density in the corona is more complex. A number of coronal density models have been derived from analyses of white-light observations (Newkirk 1961, 1967; Saito 1970; Saito et al. 1977) and from radio observations (Fainberg & Stone 1971; Leblanc et al. 1998). Each of these models, which have different ranges of validity, have distinct advantages and disadvantages, depending on the particular application.

The Saito et al. (1977) model has the approximate $1/R^2$ falloff (actually $1/R^{2.14}$) for large R , but it has the disadvantage of being valid no closer to the Sun than about $2.5 R_{\odot}$. The Leblanc et al. (1998) model, derived from the radio observations, has a similar limitation. By contrast, the K-corona model of Saito (1970) was derived from measurements made from 1 to $4 R_{\odot}$ or so. However, since at large R the Saito (1970) model scales as $1/R^{2.5}$, rather than as $1/R^2$, it is only approximately valid for distances far from the Sun. For the type II and type III radio observations to be analyzed here, which range in frequency from hundreds of MHz to ~ 500 kHz, we require a coronal density model that is valid from about 1.2 to $\sim 20 R_{\odot}$. Therefore, the Saito (1970) model is the best choice of density model for the present application, even though it is not precisely valid out as far as $20 R_{\odot}$. However, since the results and conclusions to be presented here do not depend critically on the actual density model used, this is not a serious limitation.

Type II radiation, like the type III emissions, is generated by the plasma emission mechanism, which means that the observed emission frequency is directly related to the local plasma density

in the source region: $f(\text{kHz}) = f_p = 9[n_p(\text{cm}^{-3})]^{1/2}$ for fundamental emission and $f(\text{kHz}) = 2f_p$ for harmonic emission. Using this relationship, together with the coronal density model, the height-time data displayed in Figure 4 can be readily converted to a corresponding frequency-time relationship that characterizes the kinematics of the CME.

Although the radial distance falloff of the plasma density in the corona is reasonably well described by the Saito (1970) model, the overall scale factor of this density-distance relationship can vary significantly due to the usual temporal and spatial density variations in the corona and interplanetary space. While the origin time and the overall shape of these frequency-time curves are fixed by the CME height-time data in Figure 4, this scale factor can be varied to try to obtain a best fit to the observed frequency-drift of the kilometric type II emissions below 1 MHz in Figure 1*b*. Assuming a constant CME speed and that the observed kilometric type II emissions were generated at the fundamental of the plasma frequency, we found that the derived frequency-time curves yielded a good fit to the observed frequency drift of the type II emissions provided that we multiplied the Saito (1970) model density by an overall scale factor of 2.5. The solid white curves in Figure 1*b* show this best fit solution of the CME height-time data to the observed frequency drift of the type II emissions. Two frequency-time curves are obtained that represent the kinematics of the CME: they correspond to radio emissions generated at the fundamental and harmonic of the plasma frequency. The dashed white curves in Figure 1*b* are the frequency-time curves that represent the uncertainties in the height-time fit, displayed by the dashed lines in Figure 4. Although they differ more significantly at high frequencies (Fig. 2), all of these curves provide a good fit to the frequency drift of the broad band of kilometric type II emissions in Figure 1*b*.

These results imply that the type II radio emissions were generated in an enhanced density region, consistent with previous analyses (Robinson & Stewart 1985). As often happens, the LASCO images reveal that as this CME was propelled through the solar corona, it displaced dense streamers on either side of it; the CME-driven shock propagating through these dense streamers could then be the actual source region of the type II radiation (e.g., see Reiner et al. 2003).

To relate the high- and low-frequency coronal phenomena to the CME, the solid white curves on Figures 2*a* and 2*b* show the extension, to frequencies above 1 MHz, of the frequency-time track of the CME, derived from the 2.5x Saito (1970) coronal density model. The projected liftoff time of the CME (00:27.1 \pm 00:02 UT) corresponds, to within the estimated uncertainties, to the onset of the impulsive phase of the RHESSI HXR event and to the observed sudden increase in the 5.1–17.1 GHz dm–cm radio flux.

It is particularly notable that this CME frequency-time track passes directly through the region of diminished type III-like emissions from \sim 3 to 14 MHz, suggesting that these weaker type III-like emissions directly relate to the kinematics of the CME implied by the observed height-time values. This is the first quantitative observational evidence that the CME may be responsible for the diminished type III radiation, at least for this event. The fact that some of the type III emissions extend to frequencies higher than the metric type II emissions also suggests that the type III-like emissions were not generated from electrons accelerated by the CME-driven shock, but rather by electrons accelerated deeper in the corona (Dulk et al. 2000; Cane et al. 2002).

While no dekametric type II emissions were evident along the frequency-time track of the CME during the time of the dimin-

ished type III emissions, the weak kilometric type II emissions were clearly visible up to the highest RAD1 frequency of 1 MHz and there was some hint of such emissions in the RAD2 band after the end of the intense type III emissions (see Fig. 1*b*). However, weak type II emissions may also have been generated at frequencies above 1 MHz during the time of the complex type III-like emissions, but, due to the lower sensitivity of the RAD2 receiver/antenna system and to the presence of the more intense type III-like emissions in this frequency range, the weak type II emissions were not detectable during this time, despite the fact that the type III radiation was greatly diminished.

Since the (projected) height of the CME at any time is known, from the height-time data in Figure 4, the simultaneous fit of the frequency drift of the type II radio emissions to the CME kinematics provides an estimate of the coronal height of a radio source observed at any given frequency. If it is assumed that all the relevant observed solar radio emissions associated with this event were generated within the corona described by the 2.5x Saito (1970) model, then the coronal height of any radio source at any given frequency is determined; these scale heights are indicated on the right scale on the dynamic spectra in Figure 2.

3.4. Metric Type II Emissions

Metric emissions between 00:29 and 00:35 UT, shown in Figure 2*b*, represent an admixture of type II and type III emission features. The metric type II emissions, shown in greater detail on the HiRAS dynamic spectrum in Figure 3*a*, exhibit a complex split-band structure. The frequency-time track of the CME extends through this region of complex metric emissions. While the complexity of these emissions make a clear association with specific metric features somewhat problematic, this track does qualitatively follow the frequency drift of some of the intense metric emission features observed below 100 MHz, suggesting that some of the metric type II-like emissions may have been generated by the shock driven by the CME, while the CME was still very low in the corona (\sim 1.3 R_\odot). The formation of a MHD shock in the corona depends on the characteristic Alfvén speed profile (Mann et al. 1999, 2003; Gopalswamy et al. 2001). A shock may form as the CME propagates through a region of the corona that has an Alfvén speed lower than the propagation speed of the CME. The very high speed of the 2002 July 23 CME increases the likelihood of regions favorable to shock formation in the low corona, which may therefore be the source of some of the metric type II-like emissions.

Nevertheless, it is evident that the majority of the intense, split-band type II emissions in Figures 2*b* and 3*a* exhibit frequency drift rates that differ widely from the high-frequency continuation of the frequency-time track corresponding to the coronal propagation of the observed CME. For these type II emissions to have been generated by the same CME-driven shock, they would have had to be produced in a region of significantly higher coronal density. To bring the frequency-time track of the CME into the range of the observed metric type II emissions would require increasing the scale factor of the Saito (1970) coronal density model by a factor of 50 or more. But even then the frequency-time track could not be made to fit the observed frequency drift over an extended frequency/time range.

It has been argued (Gopalswamy et al. 2000) that complex type II emissions, such as these, may have resulted from the oblique propagation of a shock, formed near the flanks of the CME. To test this hypothesis, we supposed that the corresponding coronal shock propagated from 1 R_\odot at some angle, θ , from the radial propagation direction of the CME. Then for a coronal density profile given by the Saito (1970) model, it is

straightforward to calculate the resulting frequency-time track for this obliquely propagating shock and corresponding radio source and to try to fit this track to the observed frequency drift of the metric type II emissions in Figure 2*b*. We found that although an obliquely propagating shock produced a somewhat slower frequency drift rate, it was still not possible for this CME-driven shock, propagating at 2285 km s^{-1} , to reproduce the observed frequency drift of the metric type II emissions, even for the case of an oblique shock propagating 90° from the radial direction.

The results of these analyses suggest that it is rather unlikely that the observed frequency drift of the majority of the metric type II emissions could have been produced by a shock driven by the observed CME. The observed frequency drift can only be reasonably produced by a shock (either radially or obliquely propagating) with a speed significantly less than 2285 km s^{-1} . The simplest interpretation then is that these metric type II emissions most likely originated from a slower coronal shock, which may or may not be directly related to the observed CME. Such a shock could result from the ejection of additional coronal material associated with this flare/CME event, or, alternatively, from a distinct blast-wave shock associated with the flare itself. In the latter case, it is not necessary that this latter shock should have the same origin time as the CME.

Assuming that the coronal shock that generated the metric type II emissions had an origin time coincident with the liftoff time of the CME, we found that to fit the observed frequency drift we would have to significantly reduce the propagation speed of the corresponding CME-related disturbance, with a corresponding change in the scale factor of the Saito (1970) model. The solid blue curves in Figures 2*b* and 3*a* show the frequency-time track for a coronal shock propagating through a $1.1 \times$ Saito (1970) model corona, with a speed of 500 km s^{-1} and origin time of 00:27.1 UT. These curves provide a reasonable fit to one of the split bands of the complex type II emissions observed from 00:28 to 00:35 UT, as well as to the more clearly defined drifting type II emissions observed below 50 MHz from 00:43 to 00:53 UT (at the harmonic of the plasma frequency). We found that with a shock speed significantly higher or lower than 500 km s^{-1} , we were unable to achieve a good fit to the frequency drift of the type II emissions over this entire frequency/time range, at least within the context of the Saito (1970) coronal density model.

Perhaps a somewhat better fit to the high-frequency type II emissions is obtained if we allow this shock (at 500 km s^{-1}) to propagate through the 0.7 times Saito (1970) density model at an oblique propagation angle of $\theta = 45^\circ$ from the radial propagation direction. This latter scenario corresponds to the black dashed curves in Figures 2*b* and 3*a*. Because of the complexity of these high-frequency type II emissions, we cannot clearly differentiate between these two possibilities.

If, on the other hand, we insist that the type II emissions must have been produced by a shock propagating through the same coronal density profile implied by the fit to the kilometric type II emissions generated by the CME-driven shock, i.e., the $2.5 \times$ Saito (1970) model, then to fit the frequency drift of the observed type II emissions, it is necessary to assume that the coronal shock generating these complex type II emissions originated somewhat earlier than the liftoff time of the CME. For example, the solid pink curves in Figure 3*a* correspond to a shock propagating at 610 km s^{-1} (along the radial direction), with an origin time of 00:25 UT, i.e., two minutes before the *RHESSI* HXR impulsive event and the projected liftoff time of the CME. It is perhaps significant that this time (00:25 UT) corresponds to the

brightening of the entire flaring loop in the TRACE images². This latter solution would then be interpreted as a distinct propagating coronal shock, presumably associated with the energy release during the flare, i.e., to a (blast-wave) shock not necessarily directly related to the liftoff of the CME. The fact that these metric type II emissions do not continue to frequencies lower than ~ 10 MHz might also favor this blast-wave interpretation, although even blast-wave shocks may initially be driven (Klassen et al. 1999, 2003; Klein et al. 1999). Over the frequency-time range of the observed metric type II emissions, it is not possible to distinguish this latter solution from that of the black dashed curves that correspond to the obliquely propagating shock traveling at 500 km s^{-1} through a $0.7 \times$ Saito (1970) model corona.

During the last few decades, there has been considerable debate concerning these two possibilities (for a review, see Cliver et al. 1999), which is still not satisfactorily resolved. Reiner & Kaiser (1999b) and Reiner et al. (2000a) have emphasized the importance of establishing and comparing the projected origin times. Although the above methodology offers a possible framework that may help to resolve the two-shock debate, unfortunately, the observed metric data for the July 23 event is insufficiently precise to unequivocally distinguish between these two possibilities.

We conclude from these analyses that it is most likely that the majority of the complex metric type II emissions for the 2002 July 23 event were generated by a coronal shock with a different speed, and possibly different origin time, than the CME-driven shock that produced the other metric-to-kilometric type II emissions. But we are unable to conclusively distinguish from these complex metric type II radio emissions whether the shock originated from CME-related ejecta moving at a slower speed or from a distinct shock that originated at a slightly different time.

In the scenario presented above of a separate shock originating at 00:25 UT, this coronal shock and its associated type II source would be at about $1.1 R_\odot$ at the liftoff time of the CME; in the other scenarios this latter coronal shock would be coincident with the liftoff of the CME. However, in all these scenarios the slower coronal shock, at the time of flare maximum ($\sim 00:36$ UT), would be between 1.3 and $1.6 R_\odot$, i.e., just above the large coronal loops observed in the EIT images. At this same time, the (faster) shock driven by the CME was at $2.7 R_\odot$, i.e., 3–6 times higher than the coronal shock. This makes it rather difficult to envision that the metric and kilometric type II radio emissions could all have been produced by the same CME-driven shock front, consistent with Reiner & Kaiser (1999b) and Reiner et al. (2000a).

3.5. Discussion

Reiner & Kaiser (1999a) and Reiner et al. (2001) found unusual radiation characteristics of the type III emissions in the Dm–Hm wavelength range for major energetic solar eruptive processes involving CMEs. Reiner et al. (2000b) also provided evidence, from the decimeter radio flux, that the complex type III-like emissions were related to electron acceleration low in the corona, but at that time no HXR observations were available that more directly reveals the electron acceleration event. The motivation for the present investigation was to clarify how the observed radio features, which correspond to physical phenomena high in the corona, relate to other physical processes occurring in the high and low corona, as revealed by the *RHESSI* HXR

² See http://hea-www.harvard.edu/trace/flare_catalog.

observations and the CME kinematics. The good temporal correspondence with the impulsive *RHESSI* HXR flux, together with the dm–cm emissions, further confirms that the complex type III–like radio emissions, observed at Dm–Hm wavelengths, were indeed all related to a common electron acceleration event low in the corona.

The microwave emissions are believed to be generated over a wide frequency band (see Fig. 3*b*), via the gyrosynchrotron mechanism, by (≥ 100 keV) electrons trapped in coronal loops or sets of loops, likely from the same electron beam that generated the HXR emissions when they reached the chromosphere (Bastian et al. 1998). As mentioned above, White et al. (2003) have shown that there is a striking correspondence between the spikes and dips in the *RHESSI* HXR flux (60–100 keV) and the microwave (35 GHz) intensity-time profiles over the impulsive phase of this 2002 July 23 event, consistent with a single population of accelerated electrons generating both the HXR and microwave emissions. Although the detailed resemblance becomes less obvious at lower frequencies, Figure 2*c* shows that the overall shape of the profile is maintained and that remnants of individual impulsive events are still preserved at 5.1 GHz. This observation justifies previous conclusions that the similarity of the ~ 1 MHz radio fluxes and the dm–cm radio emissions, to 4.5 GHz, implied that the complex type III–like emissions likely originate from electron beams initially accelerated deep in the corona, near the flare site (Reiner et al. 2000*b*).

The good temporal agreement of the onsets of the impulsive phase of the *RHESSI* HXR, the intense dm–cm radio emissions, and the Dm–Hm type III emissions with the projected liftoff time of the CME is also significant. It suggests that the electron acceleration event may have been triggered by magnetic reconnection that accompanied the liftoff of the CME (Maia & Pick 2004; Klein et al. 2005).

Ordinary type III radio bursts radiate continuously as the electron beam propagates outward along the Parker spiral magnetic field lines, which are more or less uniform and undisturbed from the Sun to 1 AU (Fainberg et al. 1972; Reiner et al. 1995). For such bursts the intensity of the radiation is approximately uniform across the Dm–Hm band (Hartz 1969; Reiner & Kaiser 1999*a*). By contrast, for the complex type III–like bursts that involve major coronal eruptions, the magnetic field lines are likely highly distorted in the region of the CME/shock. Furthermore, the type III electron beam may propagate through the turbulent region of the CME and/or its associated shock, which latter likely extends beyond the limits of the CME driver (Kennel et al. 1982). Either of these possibilities may destroy the bump-on-tail instability that leads to the generation of the radio emissions, thus explaining the diminished Dm–Hm radio emissions. At lower frequencies (≤ 3 MHz), corresponding to heliocentric distances above the CME/shock, the individual type III emission substructures intensify and coalesce to form intense type III–like emissions that extend to very low frequencies (see Fig. 1*b*), as the bump-on-tail instability presumably reforms beyond the turbulent region of the CME/shock. This explains why the intensity profile of the radio emissions near 1 MHz is qualitatively similar to that at dm–cm wavelengths.

4. CONCLUSION

For the 2002 July 23 solar event, by relating the low-frequency type II drift rate to the CME kinematics, we were able to establish, within the context of the Saito (1970) coronal density model, a quantitative connection between the high coronal phenomena (low-frequency radio emissions and white-light CME)

and the low corona phenomena (high-frequency radio and soft and hard X-ray emissions). Our conclusions are summarized below.

1. We found that the linearly extrapolated liftoff time of the CME (to within the uncertainties) occurs precisely at the onset times of the intense impulsive-phase HXR event and the metric and dekametric type III–like emissions, suggesting that reconnection associated with the liftoff of the CME may be responsible for the acceleration of the electrons that produced these various radio and X-ray signatures.

2. We found that the temporal behavior and duration of the flux density of the hectometric type III–like emissions correlate well with the dm–cm radio emissions (5.1–17.1 GHz) and with the impulsive-phase HXR flux. This suggests that for this July 23 event a single coronal acceleration process, which produced the downward propagating electrons that generated the HXR and dm–cm radio emissions, also produced the outward propagating electron beams that escaped into the interplanetary medium to produce the complex type III–like emissions.

3. At Dm–Hm wavelengths, the frequency-time track that corresponds to the kinematics of the CME traverses the frequency band where the complex type III–like emissions exhibited diminished radiation intensities, suggesting that the exciter electrons, which were accelerated low in the corona, lost their ability to generate radio emissions via the bump-on-tail instability, likely due to the traversal of these electrons through the turbulent region in the vicinity of the overlying CME and its associated shock wave.

4. We found that some of the frequency-drifting metric type II emissions appeared to be the high-frequency continuation of the kilometric type II emissions that were generated by the CME shock, while other metric type II emissions associated with this event were inconsistent with this origin, suggesting that additional (slower) coronal shocks are required to explain the observations. Using model calculations, we concluded that it was unlikely that the metric type II emissions were produced by obliquely propagating shocks at the flanks of the CME.

5. Since we were able from these analyses to derive an altitude scale from the simultaneous fit to the radio and white-light data, we obtained an estimate of the coronal altitude of the various radio signatures and therefore of their associated coronal shocks. For example, we estimated that at the time of flare maximum the CME-driven shock may have been 3–6 times higher in the corona than the possible flare-associated coronal shocks.

The *Wind* WAVES experiment is a collaboration of NASA/Goddard Space Flight Center, Observatoire de Paris-Meudon and the University of Minnesota. *SOHO* is an international collaboration between NASA and ESA. LASCO was constructed by a consortium of institutions: the Naval Research Laboratory (Washington, DC), the Max-Planck-Institut für Astronomie (Katlenburg-Lindau, Germany), the Laboratoire d’Astronomie Spatiale (Marseille, France), and the University of Birmingham (Birmingham, UK). M. J. R acknowledges support, in part, from the NSF grants ATM-0112186 and ATM-0417695. D. E. G. acknowledges support through NSF grant AST 03-07670 to NJIT. We thank S. Yashiro for providing the LASCO height-time data and the Hiraiso Solar Observatory for providing the metric radio spectrograph.

REFERENCES

- Bale, S. D., Reiner, M. J., Bougeret, J.-L., Kaiser, M. L., Krucker, S., Larson, D. E., & Lin, R. P. 1999, *Geophys. Res. Lett.*, 26, 1573
- Bastian, T. S., Benz, A. O., & Gary, D. E. 1998, *ARA&A*, 36, 131
- Bougeret, J. L., King, J. H., & Schwenn, R. 1984, *Sol. Phys.*, 90, 401
- Bougeret, J. L., et al. 1995, *Space Sci. Rev.*, 71, 231
- . 1998, *Geophys. Res. Lett.*, 25, 4103
- Brueckner, G. E., et al. 1995, *Sol. Phys.*, 162, 357
- Cane, H. V., Erickson, W. C., & Prestage, N. P. 2002, *J. Geophys. Res.*, 107, 1315
- Cane, H. V., Sheeley, Jr., N. R., & Howard, R. A. 1987, *J. Geophys. Res.*, 92, 9869
- Cane, H. V., & Stone, R. G. 1984, *ApJ*, 282, 339
- Cane, H. V., Stone, R. G., Fainberg, J., Stewart, R. T., Steinberg, J. L., & Hoang, S. 1981, *Geophys. Res. Lett.*, 12, 1285
- Cliver, E. W., Webb, D. F., & Howard, R. A. 1999, *Sol. Phys.*, 187, 89
- Dennis, B. R., & Zarro, D. M. 1993, *Sol. Phys.*, 146, 177
- Dougherty, B. L., Freely, W. B., Zirin, H., Gary, D. E., & Hurford, G. J. 2000, in *ASP Conf. Ser. 206, High Energy Solar Physics: Anticipating HESSI*, ed. R. Ramaty & N. Mandzhavidze (San Francisco: ASP), 367
- Dulk, G. A., Leblanc, Y., Bastion, T. S., & Bougeret, J.-L. 2000, *J. Geophys. Res.*, 105, 27343
- Fainberg, J., Evans, L. G., & Stone, R. G. 1972, *Science*, 178, 743
- Fainberg, J., & Stone, R. G. 1971, *Sol. Phys.*, 17, 392
- Gopalswamy, N., Kaiser, M. L., Sato, J., & Pick, M. 2000, in *ASP Conf. Ser. 206, High Energy Solar Physics*, ed. R. Ramaty & N. Mandzhavidze (San Francisco: ASP), 351
- Gopalswamy, N., et al. 2001, *J. Geophys. Res.*, 106, 25261
- Gurnett, D. A. 1975, *J. Geophys. Res.*, 80, 2751
- Hartz, T. R. 1969, *Planet Space Sci.* 17, 267
- Kahler, S. W., Cliver, E. W., & Cane, H. V. 1986, *Adv. Space Res.*, 6, 319
- . 1989, *Sol. Phys.*, 120, 393
- Kennel, C. F., Scarf, F. L., Coroniti, F. V., Smith, E. J., & D. A. Gurnett, 1982, *J. Geophys. Res.*, 87, 17
- Kondo, T., Isobe, T., Igi, S., Watari, S., & Tokumaru, M. 1995, *J. Commun. Res. Lab.* 42, 111
- Klassen, A., Aurass, H., & Klein, K.-L. 1999, *A&A*, 343, 287
- Klassen, A., Pohjolainen, S., & Klein, K.-L. 2003, *Sol. Phys.*, 218, 197
- Klein, K.-L., Khan, J. I., Vilmer, N., Delouis, J.-M., & Aurass, H. 1999, *A&A*, 346, L53
- Klein, K.-L., Krucker, S., Trottet, G., & Hoang, S. 2005, *A&A*, 431, 1047
- Krucker, S., Hurford, G. J., & Lin, R. P. 2003, *ApJ*, 595, L103
- Kundu, M. R., MacDowall, R. J., & Stone, R. G. 1990, *Astrophys. & Space Sci.*, 165, 101
- Kundu, M. R., & Stone, R. G. 1984, *Adv. Space Res.*, 4, 261
- Leblanc, Y., Dulk, G. A., & Bougeret, J.-L. 1998, *Sol. Phys.*, 183, 165
- Lin, R. P., et al. 2002, *Sol. Phys.*, 210, 3
- . 2003, *ApJ*, 595, L69
- MacDowall, R. J., Stone, R. G., & Kundu, M. R. 1987, *Sol. Phys.*, 111, 397
- Maia, D. J. F., & Pick, M. 2004, *ApJ*, 609, 1082
- Mann, G., Aurass, H., Klassen, A., Estel, C., & Thompson, B. J. 1999, 8th SOHO Workshop, ed. J.-C. Vial & B. Kaldeich-Schumann (SP-446; ESA: Paris), 477
- Mann, G., Klassen, A., Aurass, H., & Classen, H. T. 2003, in *AIP Conf. Proc. 679, Solar Wind 10*, ed. M. Velli, R. Bruno, & F. Malara (Melville: AIP), 612
- Neupert, W. M. 1968, *ApJ*, 153, L59
- Newkirk, G., Jr. 1961, *ApJ*, 133, 983
- . 1967, *ARA&A*, 5, 213
- Reiner, M. J., Fainberg, J., & Stone, R. G. 1995, *Science*, 270, 461
- Reiner, M. J., & Kaiser, M. L. 1999a, *Geophys. Res. Lett.*, 26, 397
- . 1999b, *J. Geophys. Res.*, 104, 16979
- Reiner, M. J., Kaiser, M. L., & Bougeret, J.-L. 2001, *J. Geophys. Res.*, 106, 29989
- Reiner, M. J., Kaiser, M. L., Fainberg, J., & Stone, R. G. 1998, *J. Geophys. Res.*, 103, 29651
- Reiner, M. J., Kaiser, M. L., Plunkett, S. P., Prestage, N. P., & Manning, R. 2000a, *ApJ*, 529, L53
- Reiner, M. J., Karlický, M., Jiříčka, K., Aurass, H., Mann, G., & Kaiser, M. L. 2000b, *ApJ*, 530, 1049
- Reiner, M. J., Vourlidas, A., St. Cyr, O. C., Burkepile, J. T., Howard, R. A., Kaiser, M. L., Prestage, N. P., & Bougeret, J.-L. 2003, *ApJ*, 546, 533
- Robinson, R. D., & Stewart, R. T. 1985, *Sol. Phys.*, 97, 145
- Saito, K. 1970, *Annu. Tokyo Astron. Obs.*, Ser. 2, 12, 53
- Saito, K., Poland, A. I., & Munro, R. H. 1977, *Sol. Phys.*, 55, 121
- St. Cyr, O. C., Burkepile, J. T., Hundhausen, A. J., & Lecinski, A. R. 1999, *J. Geophys. Res.*, 104, 12493
- White, S. M., Krucker, S., Shibasaki, K., Yokoyama, Shimojo, M., & Kundu, M. R. 2003, *ApJ*, 595, L111